An augmented-space recursion study of the electronic structure of rough epitaxial overlayers

1998 J. Phys.: Condens. Matter 10 5767

(http://iopscience.iop.org/0953-8984/10/26/005)

J. Phys.: Condens. Matter **10** (1998) 5767–5779. Printed in the UK PII: S0953-8984(98)90836-0

An augmented-space recursion study of the electronic structure of rough epitaxial overlayers

Biplab Sanyal†, Parthapratim Biswas†, A Mookerjee†,
Hemant G Salunke‡, G P Das‡ and A K Bhattacharyya§

† S N Bose National Centre for Basic Sciences, JD Block, Sector 3, Salt Lake City, Calcutta 700091, India

‡ Bhabha Atomic Research Centre, Trombay, Mumbai, India

§ Centre for Catalysis and Materials Studies, Department of Engineering, University of Warwick, Coventry, UK

Received 19 January 1998

Abstract. In this communication we propose the use of the augmented-space recursion as an ideal methodology for the study of electronic and magnetic structures of rough surfaces, interfaces and overlayers. The method can take into account roughness, short-ranged clustering effects, surface dilatation and interdiffusion. We illustrate our method by an application to an Fe overlayer on a Ag(100) surface.

1. Introduction

Magnetism at surfaces, overlayers and interfaces has evoked much interest in recent times [1]. The chemical environment of an atom at a surface or in an overlayer is very different from that in the bulk. The difference in environment, the existence of surface states and the hybridization of the states of the overlayer with those of the substrate can give rise to a wide variety of new and interesting material and magnetic properties. This wide variety has the potential for providing the basis for surface materials design. This is the underlying reason for the absorbing theoretical interest in this field.

In this communication we wish to argue that the augmented-space recursion (ASR) introduced by us earlier is one of the most suitable techniques for the study of rough overlayers and interfaces.

First-principles all-electron techniques for the determination of the electronic structure based on the local spin-density approximation (LSDA) have made reasonably accurate quantitative calculations possible. Originally, the most popular of the methods were the parametrized tight-binding and the linear combination of atomic orbitals (LCAO) [2]. However, the facts that the parametrized Hamiltonian is, in general, never transferable and that the basis does not have sufficient variational freedom have led to the eclipse of such methods for quantitative calculations—in particular, of properties as sensitive to the assumptions as the magnetic moment. There have been attempts at resuscitating the LCAO method by introducing ideas of environment-dependent parametrization [3]. The generally accepted quantitative techniques include the augmented-plane-wave (APW) technique and its linearized version (the LAPW technique) [4] and the Korringa–Kohn–Rostoker (KKR) method and its linearized version (the LMTO method) [5]. The two basically related methods

0953-8984/98/265767+13$19.50

come both in full-potential versions, where no assumption is made about the shape of the charge density or the potential, and in spherically symmetrized muffin-tin-potential versions. The electrons may be treated either semi-relativistically or fully relativistically [6]. In addition, Andersen and co-workers [7] have proposed a tight-binding LMTO (TB-LMTO) method in which the real-space representation of the Hamiltonian is sparse. Which of the two basic methods we choose often depends on personal taste and history. Moreover, how far we wish to go down the ladder of different approximations is guided by the accuracy required and the computational burden that we wish to face. We would not like to comment on this, other than justifying the choice of the specific technique that we have chosen for ourselves.

The other important aspect of the problem is the loss of translational symmetry perpendicular to the surface. This aspect has been dealt with by different authors in different ways:

(i) finite-slab calculations, which assume that finite-size effects are negligible [8];

(ii) supercell calculations, where the translational symmetry is restored; each supercell has a replica of the finite system and the assumption is that the supercells are large enough not to affect one another;

(iii) the slab Green function method where the translational symmetry parallel to the surface is utilized and the perpendicular direction is treated in real space [9–11]; the embedding method of Inglesfield [12] belongs to this group, where the Green function of the semi-infinite solid is calculated by folding down onto this semi-infinite subspace;

(iv) the fully real-space-based recursion method [13] which does not require any translational symmetry and was originally developed for dealing with surfaces and interfaces.

Overlayers produced by molecular beam epitaxy and other vapour deposition techniques are, by and large, rough. Local probes, such as STM techniques, reveal steps, islands and pyramid-like structures. Moreover, there is always interdiffusion between the overlayer and the substrate leading to a disordered-alloy-like layer at the interface. This brings in the last important aspect of the problem: roughness or disorder parallel to the surface. A majority of the theoretical work done on surfaces and overlayers so far had always assumed flat layers. Such studies generally involve the use of surface Green functions, $G(k_{\parallel}, z)$, which allow the breaking of translational symmetry perpendicular to the surface, but presume such symmetry parallel to it [9, 10]. Roughness has been introduced in overlayers by randomly alloying them with *empty spheres* [11]. Such alloying has been assumed to be homogeneous and has been treated within a mean-field or the coherent potential approximation (CPA). Attempts at going beyond the CPA have not generally been successful. One of the more successful approaches in this direction is the augmented-space formalism (ASF) [14] and techniques basically based on it, like the travelling-cluster approximation (TCA) [15].

Let us now explain why we wish to advocate the augmented-space recursion based on the TB-LMTO as an attractive method for the study of rough surfaces, overlayers or interfaces.

The CPA has proven to be an accurate approximation in a very large body of applications. Why then do we wish to go beyond it? We should recall that the CPA is *exact* when the local coordination is infinite. Its accuracy is inversely proportional to the local coordination. We therefore expect the CPA to be less accurate at a surface as compared with the bulk calculations. Furthermore, the CPA basically describes homogeneous randomness. It cannot accurately take into account clustering, short-ranged ordering or local lattice distortions, of the kind that we expect to encounter in the rough surfaces produced experimentally. The

ASF allows us to describe such situations exactly, without violating the so-called '*herglotz*' properties which the approximated averaged Green function must possess [16].

We shall combine the ASF with the recursion method to calculate the configuration-averaged Green functions. We should note that the augmented-space theorem is *exact* [16] and that the approximation involves terminating the recursion-generated continued fraction. Analyticity-preserving 'terminators' have been introduced by Haydock and Nex [17] and Luchini and Nex [18]. Recently Ghosh *et al* [19] have discussed the convergence of the augmented-space recursion and indicated how to generate physical quantities within a prescribed error window. The recursion method, being entirely in real space, does not require any translational symmetry and is ideally suited for systems with inhomogeneous disorder. However, for the recursion method to be a practicable computational technique, we must choose a basis of representation in which the effective Hamiltonian is sparse, i.e. short ranged in real space. The best choice of a computationally simple yet accurate basis is the TB-LMTO one. This is what we describe in this communication. However, the screened KKR method [6] would be a more quantitatively accurate choice. We would require the energy-dependent extension of the recursion method. This has been developed recently [20] and its application to the screened KKR method will be described in a subsequent communication.

To illustrate the method, we shall take a well-studied example: that of Fe deposited on the (100) surface of a Ag substrate. The lattice parameter of bcc Fe, the most common ferromagnet [21], matches the nearest-neighbour distance on the (100) surface of fcc Ag (half the face diagonal), a very good non-magnetic electrical conductor. This favours epitaxial deposition of bcc Fe on Ag(100), manifesting interesting magnetic properties.

Before describing the methodology in some detail, we need to clarify the following point: in order to describe inhomogeneous disorder we have taken recourse to the generalized augmented-space theorem [22]. This generalized ASF takes into account short-ranged order through the Warren–Cowley parameter and yields an analytic *herglotz* approximation. In a recent publication [23] the authors make the unfounded statement that the generalized ASF yields negative densities of states, and quote the work of Razee and Prasad [24]. The statement is untrue and the misconception should be cleared up. A careful reading of the quoted article [24] will show that, in applying the generalized ASF, Razee and Prasad use the Nikodym–Radon transform and write the joint density of states of the Hamiltonian parameters $\mathcal{P}(\{\epsilon_i\})$ as $(\prod p(\epsilon_i))\Phi(\{\epsilon_i\})$. For homogeneous disorder, $\Phi(\{\epsilon_i\})$ is unity, while for inhomogeneous disorder, the authors expand the function as an infinite series involving various correlation functions between the $\{\epsilon_i\}$ (the simplest two-site correlation can be written in terms of the Warren–Cowley parameter). They then truncate this series after a few terms. This extra approximation cannot guarantee the preservation of the *herglotz* analytic properties and is the cause of the observed negative density of states in some energy regimes. The generalized ASF described by Mookerjee and Prasad [22] does not take recourse to such an approximation and has been shown to be exact. Approximation then arises entirely due to the recursion termination—which has been shown to preserve the *herglotz* analytic properties.

2. The generalized augmented-space theorem

In this section we shall describe the generalized augmented-space formalism. The Hamiltonian is a function of a set of random variables $\{n_i\}$ which are not independent, so the joint probability distribution can be written in terms of the conditional probability

densities of the individual variables as

$$p(\{n_i\}) = p(n_1)\prod_k p(n_k|n_{k-1}, n_{k-2}, \ldots, n_1).$$

Each random variable n_k has associated with it its own configuration space Φ_k and, in the case of correlated disorder, a set of operators $\{M_k^{\lambda_{k-1},\lambda_{k-2},\ldots,\lambda_1}\}$ whose spectral densities are the conditional probability densities of the random variable, dependent on the configurations of the sites labelled as superscripts. The λ_k label the configurations of the variable n_k. The configuration space of the set of random variables is the product $\Psi = \prod_k^{\otimes} \Phi_k$. What the generalized augmented-space theorem proved was that, if we define operators on this full configuration space:

$$\tilde{M}_k = \sum_{\lambda_1}\sum_{\lambda_2}\cdots\sum_{\lambda_{k-1}} P_1^{\lambda_1}\otimes P_2^{\lambda_2}\otimes\cdots\otimes P_{k-1}^{\lambda_{k-1}}\otimes M_k^{\lambda_{k-1},\lambda_{k-2},\ldots,\lambda_1}\otimes I\otimes I\cdots$$

then the configuration average of any function of the Hamiltonian is given *exactly* by

$$\langle\langle\mathcal{F}(\{n_k\})\rangle\rangle = \langle F^0|\tilde{\mathcal{F}}(\{\tilde{M}_k\})|F^0\rangle. \tag{1}$$

The average state $|F^0\rangle$ is defined by

$$|F^0\rangle = \prod_k |f_k^0\rangle$$

$$|f_k^0\rangle = \sum_{\lambda_k}\sqrt{\omega_{\lambda_k}^{\lambda_1,\lambda_2,\ldots,\lambda_{k-1}}}\,|\lambda_k\rangle$$

where the numbers under the root sign are the conditional probability weights for the various configurations of the variable n_k.

In our model, the random variables are the variables describing occupation of a site by two different kinds of atom. The simplest model is one that assumes that the occupation of the nearest neighbours of a site depends on its own occupation. The probability densities are given by

$$p(n_1) = x\delta(n_1 - 1) + y\delta(n_1)$$

$$p(n_2|n_1 = 1) = (x + \alpha y)\delta(n_2 - 1) + (1 - \alpha)y\delta(n_2)$$

$$p(n_2|n_1 = 0) = (1 - \alpha)x\delta(n_2 - 1) + (y + \alpha x)\delta(n_2)$$

where x and y are the concentrations of the constituents and α is the Warren–Cowley short-range-order parameter. $\alpha = 0$ refers to the completely random case, in which the various operators $M_k^{\lambda_{k-1},\ldots,\lambda_1}$ become independent of the superscripts and the generalized augmented-space theorem reduces to the usual augmented-space theorem. $\alpha < 0$ indicates the tendency towards ordering alternately, while $\alpha > 0$ indicates the tendency towards segregation.

The representations of the corresponding operators required are the following:

$$\mathbf{M}_1 = \begin{pmatrix} x & \sqrt{xy} \\ \sqrt{xy} & y \end{pmatrix}$$

$$\mathbf{M}_2^1 = \begin{pmatrix} x + \alpha y & \sqrt{(1-\alpha)y(x+\alpha y)} \\ \sqrt{(1-\alpha)y(x+\alpha y)} & (1-\alpha)y \end{pmatrix}$$

$$\mathbf{M}_2^0 = \begin{pmatrix} (1-\alpha)x & \sqrt{(1-\alpha)x(y+\alpha x)} \\ \sqrt{(1-\alpha)x(y+\alpha x)} & y + \alpha x \end{pmatrix}$$

$$\mathbf{P}_1^0 = \begin{pmatrix} x & \sqrt{xy} \\ \sqrt{xy} & y \end{pmatrix}$$

$$\mathbf{P}_1^1 = \begin{pmatrix} y & -\sqrt{xy} \\ -\sqrt{xy} & x \end{pmatrix}.$$

3. The TB-LMTO-ASR formulation

Our system consists of a semi-infinite Ag substrate with layers of Fe atoms on the (100) surface. We shall describe the Hamiltonian of the electrons within a tight-binding linearized muffin-tin orbital (TB-LMTO) basis. As described earlier, we shall circumvent the problem of the charge leakage into the vacuum by introducing layers of empty spheres containing charge but no atoms. We shall roughen the topmost layer by randomly alloying the Fe atoms with empty spheres. We shall allow for short-ranged order in the alloying. Segregation will imply that the Fe atoms and empty spheres cluster together forming islands and clumps. Ordering on the other hand will imply that Fe atoms 'like' to be surrounded by empty spheres and vice versa.

Extensive details of the description of the effective augmented-space Hamiltonian have been given in an earlier paper [25]. We shall indicate the generalization of the result for the cases where nearest-neighbour short-ranged order is introduced as described above:

$$\begin{aligned}\tilde{H} = {} & \mathbf{H}_1\tilde{\mathbf{I}} + \mathbf{H}_2\sum_k \mathbf{P}_k \otimes \mathbf{P}^k_{\downarrow} + \mathbf{H}_3\sum_k \mathbf{P}_k \otimes \{\mathbf{T}^k_{\downarrow\uparrow} + \mathbf{T}^k_{\uparrow\downarrow}\} \\ & + \mathbf{H}_4\sum_k\sum_{k'} \mathbf{T}_{kk'} \otimes \mathbf{I} + +\alpha\mathbf{H}_2\sum_{m\in N_1} \mathbf{P}_m \otimes \mathbf{P}^1_{\downarrow} \otimes \{\mathbf{P}^m_{\uparrow} - \mathbf{P}^m_{\downarrow}\} \\ & + \mathbf{H}_5\sum_{m\in N_1} \mathbf{P}_m \otimes \mathbf{P}^1_{\uparrow} \otimes \{\mathbf{T}^m_{\uparrow\downarrow} + \mathbf{T}^m_{\downarrow\uparrow}\} + \mathbf{H}_6\sum_{m\in N_1} \mathbf{P}_m \otimes \mathbf{P}^1_{\downarrow} \otimes \{\mathbf{T}^m_{\uparrow\downarrow} + \mathbf{T}^m_{\downarrow\uparrow}\} \\ & + \alpha\mathbf{H}_2\sum_{m\in N_1} \mathbf{P}_m \otimes \{\mathbf{T}^1_{\uparrow\downarrow} + \mathbf{T}^1_{\downarrow\uparrow}\} \otimes \{\mathbf{P}^m_{\uparrow} - \mathbf{P}^m_{\downarrow}\} \\ & + \mathbf{H}_7\sum_{m\in N_1} \mathbf{P}_m \otimes \{\mathbf{T}^1_{\uparrow\downarrow} + \mathbf{T}^1_{\downarrow\uparrow}\} \otimes \{\mathbf{T}^2_{\uparrow\downarrow} + \mathbf{T}^2_{\downarrow\uparrow}\} \end{aligned} \tag{2}$$

where N_1 is the set of nearest neighbours of the site labelled 1 on the surface, and for calculations of the averaged local densities of states at a constituent labelled λ we have

$$\begin{aligned}
\mathbf{H}_1 &= A(\mathbf{C}/\boldsymbol{\Delta})\boldsymbol{\Delta}_\lambda - (EA(1/\boldsymbol{\Delta})\boldsymbol{\Delta}_\lambda - 1) \\
\mathbf{H}_2 &= B(\mathbf{C}/\boldsymbol{\Delta})\boldsymbol{\Delta}_\lambda - EB(1/\boldsymbol{\Delta})\boldsymbol{\Delta}_\lambda \\
\mathbf{H}_3 &= F(\mathbf{C}/\boldsymbol{\Delta})\boldsymbol{\Delta}_\lambda - EF(1/\boldsymbol{\Delta})\boldsymbol{\Delta}_\lambda \\
\mathbf{H}_4 &= (\boldsymbol{\Delta}_\lambda)^{-1/2}\mathbf{S}_{RR'}(\boldsymbol{\Delta}_\lambda)^{-1/2} \\
\mathbf{H}_5 &= F(\mathbf{C}/\boldsymbol{\Delta})\boldsymbol{\Delta}_\lambda\left[\sqrt{(1-\alpha)x(x+\alpha y)} + \sqrt{(1-\alpha)y(y+\alpha x)} - 1\right] \\
\mathbf{H}_6 &= F(\mathbf{C}/\boldsymbol{\Delta})\boldsymbol{\Delta}_\lambda\left[y\sqrt{(1-\alpha)(x+\alpha y)/x} + x\sqrt{(1-\alpha)(y+\alpha x)/y} - 1\right] \\
\mathbf{H}_7 &= F(\mathbf{C}\boldsymbol{\Delta})\boldsymbol{\Delta}_\lambda\left[\sqrt{(1-\alpha)y(x+\alpha y)} - \sqrt{(1-\alpha)x(y+\alpha x)}\right] \\
A(Z) &= xZ_A + yZ_B \\
B(Z) &= (y-x)(Z_A - Z_B) \\
F(Z) &= \sqrt{xy}(Z_A - Z_B)
\end{aligned} \tag{3}$$

$\mathbf{C}$, $\boldsymbol{\Delta}$ and $\mathbf{S}$ are matrices whose elements are angular momenta; $\mathbf{C}$ and $\boldsymbol{\Delta}$ are diagonal. We note first of all that when the short-ranged order disappears and $\alpha = 0$, the terms $\mathbf{H}_5$ to $\mathbf{H}_7$ also become zero and the Hamiltonian reduces to the standard one described earlier [25].

This effective Hamiltonian is sparse in the TB-LMTO basis, but as the expressions show, there is an energy dependence in the first three terms. This compels us to carry out recursion at every energy step. However, Ghosh *et al* [20] have shown that the corresponding energy

dependence of the continued-fraction coefficients is very weak, and if we carry out recursions at a few selected *seed* energies across the spectrum, we may obtain accurate results by spline fitting the coefficients over the spectrum.

For the self-consistent calculations we need to calculate the partial (atom-projected) densities of states at various sites in different layers. This is done by running the recursion starting from sites in different layers. We shall assume that beyond five layers from the surface, bulk values are obtained. We checked that this is indeed the case, by comparing the results for the fifth layer and those from a full bulk calculation. The Fermi energy of the system is that of the bulk substrate, which we have taken from the bulk calculations. In all cases we have used up to seven shells in augmented space and terminated the recursion after eight to ten steps of recursion. We have used the terminator proposed by Luchini and Nex [18]. As discussed in an earlier paper [19], we have made sure that the moments of the densities of states converge as the number of augmented-space shells and recursions increase to within a preassigned error range, which is consistent with the errors in the TB-LMTO approximations. We have made the recursive calculations LDA self-consistent. For this we had to obtain the radial solutions of the Schrödinger equation involving the spherically symmetric LDA potential

$$V_p^\lambda(r) = -2\frac{Z^\lambda}{r} + V_p^{\lambda,H}\left[\rho^\lambda(r)\right] + V_p^{\lambda,XC}\left[\rho^\lambda(r)\right] + \sum_L \sum_q M_{pq}^L Q_q^L.$$

λ labels the type of atom, Z^λ labels its atomic number and p labels the particular layer. The second term in the equation is the Hartree potential, which is obtained by solving the Poisson equation with the layer- and atom-projected charge densities. The third term is the exchange–correlation term. For this term we have used the von Barth–Hedin form. In the last term,

$$Q_p^L = \sum_\lambda x_p^\lambda \left\{ \frac{\sqrt{4\pi}}{2\ell+1} \int_0^s Y_L(\hat{r})|r|^\ell \rho_p^\lambda(r)\ \mathrm{d}r - Z^\lambda \delta_{\ell,0} \right\}.$$

Here λ for the overlayer is either Fe or an empty sphere and the concentration x_p^λ is either x or $1-x$. For the substrate, λ refers only to Ag and its concentration is 1, while for the charge layers outside the overlayer, λ refers to the empty sphere and its concentration is also 1.

This last term describes the effect of redistribution of charge near the surface, which is particularly important for surface electronic structure. This charge density near the surface is far from spherically symmetric. We have taken into account both the monopole ($\ell = 0, m = 0$) and the dipole ($\ell = 1, m = 0$) contributions. We have also averaged the multipole moments in each layer and used the technique described by Skriver and Rosengaard [26] to evaluate the matrices M_{pq}^L by a Ewald technique.

4. Results and discussion

In order to compare our results with calculations carried out earlier, we shall first carry out calculations on a (100) surface of bcc Fe. Earlier, Wang and Freeman [2] used the LCAO method for the study of the same system. The FP-LAPW method had been used by Ohnishi *et al* [4] also to study the (100) surface of bcc Fe. The bulk lattice parameter was chosen (as in the case of Ohnishi *et al*) to be 5.4169 au. At this stage no lattice relaxation was considered. The results quoted below were for the semi-relativistic self-consistent

Table 1. Magnetic moments in Bohr magnetons/atom.

	S	$S-1$	$S-2$	B
Wang and Freeman	3.01	1.69	2.13	2.16
Ohnishi *et al*	2.98	2.35	2.39	2.25
Sanyal *et al* [a]	2.86	2.16	2.38	2.17
Sanyal *et al* [b]	2.99	2.17	2.38	2.27

[a] Supercell calculations.
[b] ASR calculations.

LSDA TB-LMTO technique in both the supercell and ASR versions. Table 1 compares the magnetic moment per atom for the three different methods quoted above.

Our central-layer magnetic moment per atom is close to the bulk value given by Wang and Freeman and slightly lower than that given by Ohnishi *et al*. All three methods find Friedel oscillations to be exhibited by the magnetic moment, although the oscillations found by Wang and Freeman are larger than those found by Ohnishi *et al* and than those found in our work. Our magnetic moment at the surface layer is rather small as compared to those found in the earlier work. However, in these initial calculations (marked with superscript a in the table) we have not taken into account surface relaxation. Local lattice relaxation can easily be taken into account within the TB-LMTO-ASR in [27]. We refer the reader to the details of the relaxation method given therein. A 7–8% relaxation of the surface layer leads to a surface magnetic moment of 2.99 μ_B/atom which is in good agreement with the results of both of the earlier studies (marked with superscript b in table 1).

We shall now turn to the study of Fe(100) on the (100) surface of a fcc Ag substrate. We shall carry out the calculations using two different techniques. First, we shall use the tight-binding linearized muffin-tin orbital (TB-LMTO) method with a minimal (s, p, d) basis set for Fe and Ag sites in a tetragonal supercell. Both spin-polarized and non-spin-polarized calculations were performed on an Fe/Ag multilayer containing a monolayer of Fe, a monolayer of empty spheres above them and four Ag layers as the substrate. The empty spheres solve the problem of charge leakage into the vacuum across the free surface. The results of the calculation show that spin polarization yields a total ground-state energy lower, as compared with the unpolarized case, by $\sim$0.092 eV/atom, suggesting that the ground state is magnetic. All of the Fe layers have ferromagnetically arranged moments, with interface Fe layers having a magnetic moment of $\sim$2.86 μ_B (bulk value: 2.27 μ_B). Also, Fe induces a ferromagnetic moment in Ag at the interface of $\sim$0.012 μ_B per atom. The calculation also suggests Friedel oscillations in the net valence charge in Ag as one goes from the interface to the bulk in Ag. This is because of moment spillage into the empty spheres. Such moment spillage outside the surface has also been observed by Ohnishi *et al* [4].

We shall refine our calculations in three steps. First we shall introduce the local lattice relaxation technique within the TB-LMTO-ASR [27] to relax the surface layer. We shall inflate the interlayer distance between the surface layer and the one just below it. Figure 1 shows the variation of the magnetic moment at the surface layer as a function of the percentage lattice dilatation at the surface. The minimum of the total energy occurs at around 7.5% dilatation. Here the moment carried by the monolayer of Fe is 3.17 μ_B/atom, which is not very far from the value of 3.1 μ_B/atom quoted by Blügel which was based on FP-LAPW calculations [28].

Next we shall begin with a planar monolayer of Fe on Ag and roughen the monolayer by alloying it with empty spheres. We shall now use the self-consistent ASR for obtaining

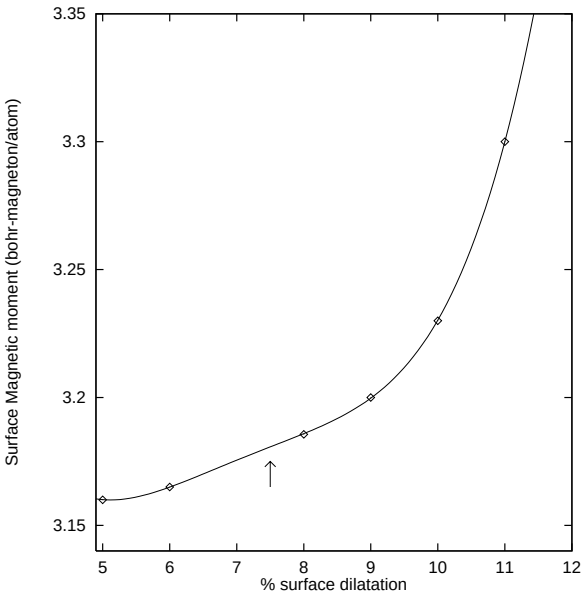

Figure 1. The surface magnetic moment (in Bohr magnetons/atom) as a function of the percentage surface dilatation (the dilatation of the distance between the surface overlayer and the next layer in the substrate).

the electronic density of states and local magnetization as a function of the concentration of the alloying and the short-range order parameter. We shall begin the LDA self-consistency procedure by using, to start with, the converged potential parameters from the supercell calculations on planar surfaces and the equilibrium lattice distances, i.e. with a 7.5% surface lattice dilatation. With this starting point, the self-consistency is reached much more quickly.

Figure 2(a) shows the local density of states at a point in the bulk Ag substrate (full lines) and that for a Ag atom on the 100 surface of fcc Ag (without the deposited Fe overlayer) (dotted lines), obtained by an eight-step recursion process. We have checked that the recursion does converge in the sense suggested by Haydock [13] and Ghosh *et al* [19] of the convergence of integrals of the form

$$\int_{-\infty}^{E} \Phi(E')n(E')\,\mathrm{d}E'$$

where $\Phi(E)$ is a well-behaved, monotonic function in the integration range. The Fermi energy or the chemical potential is calculated from the bulk, and this is shown in figure 2(a). As expected, the d-band width can be observed to decrease at the surface. This is expected, as the surface atoms are less coordinated than the bulk atoms (eightfold coordination on the 100 surface as against twelvefold coordination in the bulk). There is also a redistribution of the spectral weight in the band. It is clear that the amount of charge in a Wigner–Seitz sphere around a surface atom is less than that around a bulk atom. This extra charge leaks out into the so-called empty spheres, which carry no atoms but just this leaked charge. By the time we go down to about four layers below the surface, we begin to get local densities indistinguishable from the bulk results.

Figure 2(b) shows the local density of states for the up-spin and down-spin electrons in the Fe overlayer. This is for a perfectly planar overlayer on the 100 surface. As is usual in bulk Fe and Fe overlayers on noble metals, the majority occupied spin band (here, the

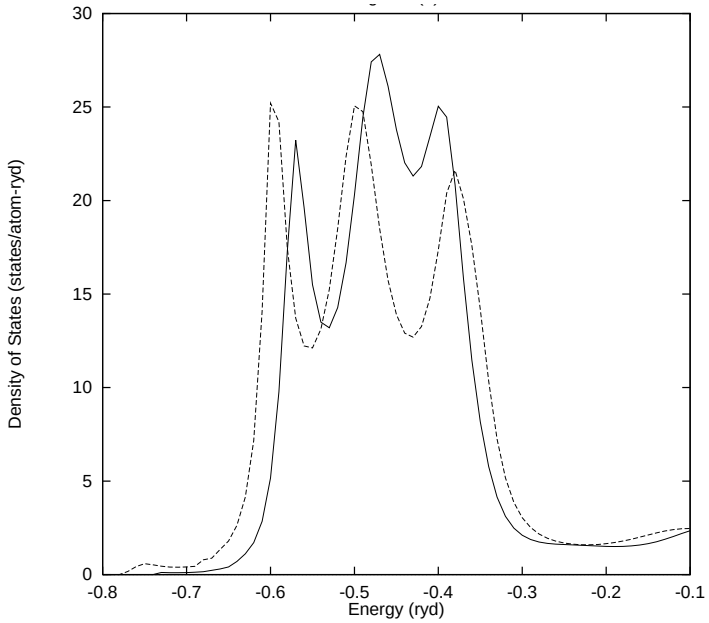

(a)

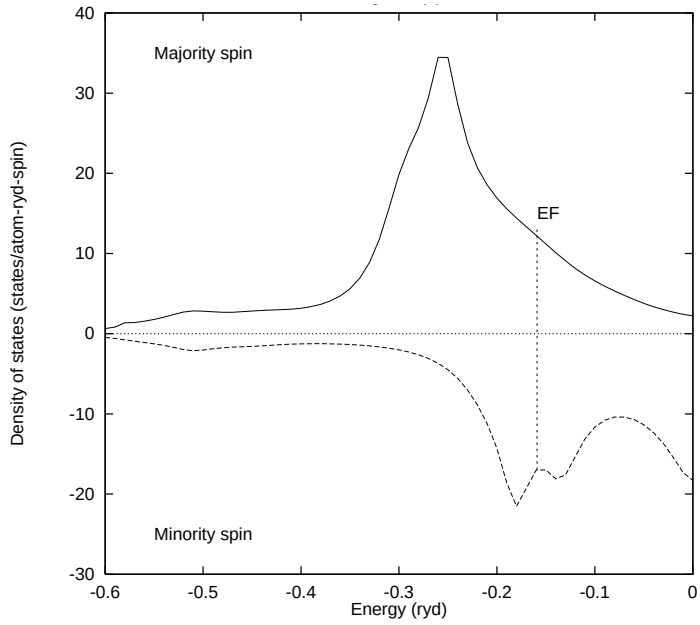

(b)

Figure 2. (a) The local density of states at a Ag atom in the bulk (dotted line) and on the (100) surface (full lines). (b) The local density of states at an Fe atom in an overlayer on the (100) surface of a Ag substrate. Both the up-spin and the down-spin densities are shown.

up-spin band) shows much more structure than the minority occupied one (here, the down-spin band). Since the Ag d bands centred around -0.5 Ryd do not overlap with either of

the Fe d bands at around −0.2 Ryd and −0.1 Ryd, there is no significant hybridization of these two, which usually leads to a widening of the Fe d bands and a consequent lowering of the local magnetic moment. The Fermi energy is that of the bulk Ag and is shown in the figure.

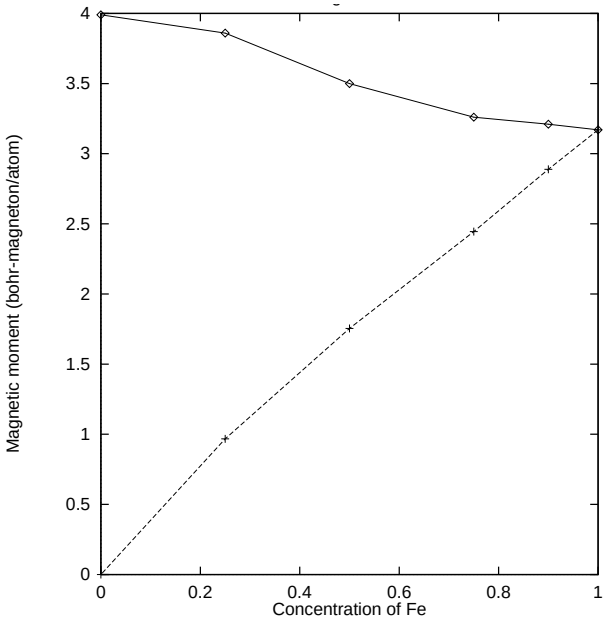

Figure 3. The local magnetic moment (dotted line) and averaged magnetic moment (full line) on an Fe atom in a rough overlayer on the (100) surface of a Ag substrate. The roughness is modelled by an alloy of Fe and empty spheres. The magnetic moments are shown as a function of the concentration of Fe in this model alloy. The results are for 7.5% surface dilatation.

We now alloy the overlayer with empty spheres and reconverge the self-consistent ASR. In figure 3 we show the local magnetic moment on an Fe atom in the rough overlayer as a function of the Fe concentration in that layer (the dotted line) with 7.5% surface dilatation. For a concentration $x = 1$ of Fe we obtain the local magnetic moment corresponding to that of figure 2(b). The value of 3.17 μ_B/atom represents a considerable enhancement as compared with the bulk bcc iron local magnetic moment. The agreement with the supercell calculations is very close. Blügel has argued [28] that this can be inferred from the Stoner criterion, because of the narrowing of the overlayer d bands as compared with the bulk. As we alloy the overlayer with empty spheres, the local magnetic moment on an Fe atom increases, until in the extreme case it approaches that of an isolated Fe atom at >3.6 μ_B/atom. Again we can understand this to a large degree from Blügel's argument. We find that the empty spheres hardly inherit any induced magnetization; as a result, as the concentration of empty spheres increases, the average coordination of Fe atoms decreases, thus increasing the magnetic moment. In the extreme limit, we obtain the case of an Fe impurity atom sitting in a sea of empty spheres. Its magnetic moment approaches that of a free Fe atom. The only difference is caused by its hybridization with the Ag substrate. Figure 3 also shows (full lines) the averaged magnetization in the overlayer. This is defined by $xM_{\mathrm{Fe}} + yM_{\mathrm{ES}}$. Since M_{ES} is negligible, this average overlayer magnetization decreases almost linearly with x and vanishes at $x = 0$. The two types of magnetization shown in the

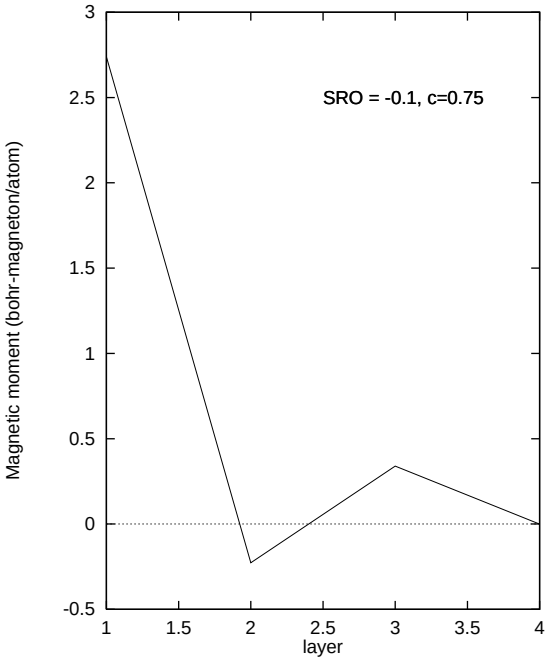

Figure 4. The oscillation of the magnetic moment on different layers of an Fe overlayer on the (100) surface of a Ag substrate.

figure are measured by local magnetic probes and global magnetization experiments.

Figure 4 shows the local magnetization at atoms in different layers. We clearly see that there is an induced magnetization in the Ag atoms of the topmost substrate layers. The magnetization oscillates layerwise into the bulk.

Figure 5 shows the variation of the local magnetic moment at an Fe site (the dotted line) and the averaged magnetic moment in the overlayer as a function of the Warren–Cowley short-range-order parameter for (a) $x = 0.9$ and (b) $x = 0.75$. We note that when the Warren–Cowley parameter indicates phase segregation, the magnetic moment shows an increase. We may understand this behaviour from the following argument.

For $\alpha > 0$ the tendency is towards phase segregation. Islands of Fe (in our case, clusters of nearest-neighbour atoms) precipitate in a sea of empty spheres (particularly in the low-Fe-concentration regime). This situation mimics the islands and pyramids observed for actual MBE-deposited surfaces. A simple calculation with an isolated five-atom nearest-neighbour cluster present on the surface shows that the local density of states in the cluster is much narrower than a homogeneous distribution of Fe atoms on the surface. This leads to a larger magnetic moment/atom on the cluster. The maximum enhancement of the magnetic moment due to short-ranged clustering is around 3%.

Clustering enhancement of the magnetic moment competes with the 'poisoning' effect. The interfaces are never sharp; there is always an interdiffusion of substrate atoms into the surface layer and vice versa. In our final calculation, we have taken a perfectly planar (non-rough) monolayer of Fe on the (100) surface of fcc Ag and allowed up to 10% interdiffusion of Fe and Ag atoms into the surface layer and the one just below it. The surface layer is then an Fe_xAg_{1-x} alloy and the next layer a Ag_xFe_{1-x} alloy. The following table, table 2, shows the magnetic moments in the surface layer for different values of x.

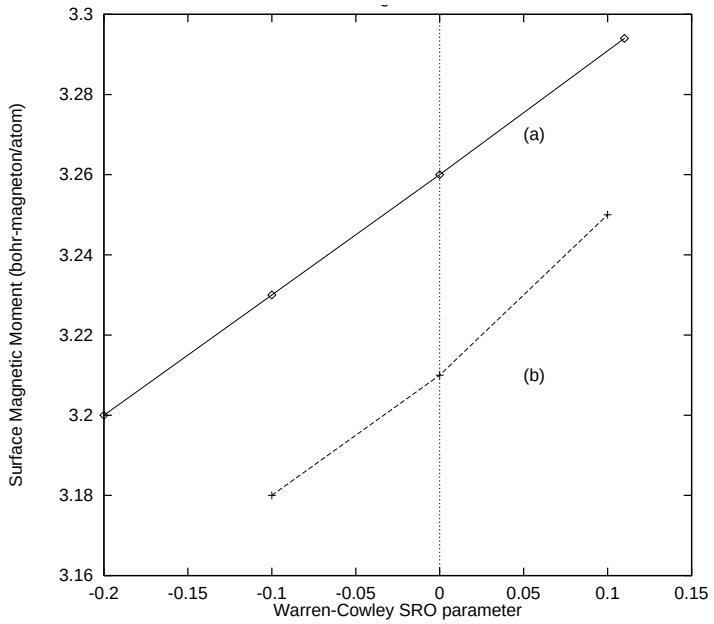

Figure 5. The surface magnetic moment (in Bohr magnetons/atom) as a function of the Warren–Cowley short-range-order parameter for (a) 90% Fe, 10% empty spheres and (b) 75% Fe, 25% empty spheres in the surface overlayer, with 7.5% surface dilatation.

Table 2. The lowering of the surface magnetism due to the 'poisoning' by the substrate. All of the magnetic moments are in μ_B/atom.

x	Averaged magnetic moment	Fe magnetic moment	Ag magnetic moment
0.95	3.02	3.18	0.014
0.90	2.86	3.17	0.017

We notice that the depletion of the magnetic moment due to the 'poisoning' by the substrate is about 4.5%. In an actual experimental situation, the enhancement effects due to the surface lattice dilatation and clustering and the depletion effect due to 'poisoning' are present simultaneously. We have an idea of how to determine the lattice dilatation. Surface roughness may be probed with local techniques like STM. If we could determine the amount of interdiffusion, we would be in a position to quantitatively predict the surface magnetic moment. In conclusion, we suggest that the augmented-space recursion coupled with any first-principles and accurate technique which yields a sparse Hamiltonian representation (like the TB-LMTO or the screened KKR method) can take into account surface roughness, short-ranged clustering, surface dilatation and interdiffusion effects accurately, and it would be a useful methodology to adopt.

Acknowledgments

AM, GPD and BS would like to thank the ICTP and its Network Project and the DST, India, for financial support of this work. PB would like to thank the CSIR, India, for financial assistance. The collaborative project between the University of Warwick and the S N Bose

National Centre is also gratefully acknowledged. We would also like to thank I Dasgupta and T Saha-Dasgupta whose bulk LDA self-consistent codes formed the basis of this surface generalization.

References

[1] Feder R (ed) 1985 *Polarized Electrons in Surface Physics* (Singapore: World Scientific)
[2] Tersoff J and Falicov L M 1981 *Phys. Rev.* B **24** 754
Victoria R H, Falicov L M and Ishida S 1984 *Phys. Rev.* B **30** 3896
Pastor G M, Dorantes-Davila J and Bennemann K 1989 *Phys. Rev.* B **40** 7642
Riedinger R, Habar M, Stauffer L, Dreysse H, Leonard P and Mukherjee M 1989 *Phys. Rev.* B **39** 13 175
Dorantes-Davila J, Vega A and Pastor G 1993 *Phys. Rev.* B **47** 12 995
Wang C S and Freeman A J 1981 *Phys. Rev.* B **24** 4364
[3] Fabricius G, Llois A M, Weissman M and Khan M A 1994 *Phys. Rev.* B **49** 2121
[4] Wimmer E, Krakauer H, Weinert M and Freeman A J 1981 *Phys. Rev.* B **24** 864
Ohnishi S, Freeman A J and Weinert W 1983 *J. Magn. Magn. Mater.* **31–34** 889
Ohnishi S, Freeman A J and Weinert W 1983 *Phys. Rev.* B **28** 6741
Ohnishi S, Freeman A J and Weinert W 1984 *Phys. Rev.* B **30** 36
[5] Skriver H L 1984 *The LMTO Method* (Berlin: Springer)
Peduto P R, Frota-Pessoa S and Methfessel M S 1991 *Phys. Rev.* B **44** 13 283
Khan M A 1993 *Appl. Surf. Sci.* **65** 18
Khan M A 1993 *J. Phys. Soc. Japan* **62** 1682
[6] Szunyogh L, Újfalussy B and Weinberger P 1997 *Phys. Rev.* B **55** 14 392 and references therein
[7] Andersen O K, Jepsen O and Gloetzel D 1985 *Highlights of Condensed Matter Theory* ed F Bassani, F Fumi and M Tosi (Amsterdam: North-Holland)
Andersen O K, Jepsen O and Šob M 1991 *Electronic Structure of Metals and Alloys* ed O K Andersen, V Kumar and A Mookerjee (Singapore: World Scientific)
[8] Callaway J and Wang C S 1977 *Phys. Rev.* B **16** 1095
[9] Kudrnovský J, Wenzien B, Drchal V and Weinberger P 1991 *Phys. Rev.* B **44** 4068
[10] Kudrnovský J, Turek I, Drchal V, Weinberger P, Christensen N E and Bose S K 1992 *Phys. Rev.* B **46** 4222
[11] Ganduglia-Pirovano M V, Kudrnovský J, Turek I, Drchal V and Cohen M H 1993 *Phys. Rev.* B **48** 1870
[12] Inglesfield J E 1971 *J. Phys. C: Solid State Phys.* **4** L14
Inglesfield J E 1972 *J. Phys. F: Met. Phys.* **2** 878
Inglesfield J E 1981 *J. Phys. C: Solid State Phys.* **14** 3795
[13] Haydock R 1982 *Solid State Physics* vol 35 (New York: Academic)
[14] Mookerjee A 1973 *J. Phys. C: Solid State Phys.* **6** L205
Mookerjee A 1973 *J. Phys. C: Solid State Phys.* **6** 1340
[15] Kaplan T and Gray L J 1976 *J. Phys. C: Solid State Phys.* **9** L203
Kaplan T and Gray L J 1976 *Phys. Rev.* B **14** 3462
Kaplan T and Gray L J 1977 *Phys. Rev.* B **15** 3260
[16] Razee S A, Mookerjee A and Prasad R P 1991 *J. Phys.: Condens. Matter* **3** 3301
[17] Haydock R and Nex C M M 1984 *J. Phys. C: Solid State Phys.* **17** 4783
Haydock R and Nex C M M 1985 *J. Phys. C: Solid State Phys.* **18** 2235
[18] Luchini N U and Nex C M M 1987 *J. Phys. C: Solid State Phys.* **20** 3125
[19] Ghosh S, Das N and Mookerjee A 1997 *J. Phys.: Condens. Matter* **48** 10 701
[20] Ghosh S, Das N, Dasgupta I, Saha-Dasgupta T and Mookerjee A 1998 *Int. J. Mod. Phys.* B at press
[21] Heinrich B and Cochran J F 1993 *Adv. Phys.* **42** 523
[22] Mookerjee A and Prasad R 1993 *Phys. Rev.* B **48** 17 724
[23] Gonis A, Turchi P E A, Kudrnovský J, Drchal V and Turek I 1996 *J. Phys.: Condens. Matter* **8** 7869
[24] Razee S S and Prasad R 1993 *Phys. Rev.* B **48** 17 724
[25] Biswas P P, Sanyal B, Fakhruddin M, Halder A, Ahmed M and Mookerjee A 1995 *J. Phys.: Condens. Matter* **7** 8569
[26] Skriver H L and Rosengaard N M 1991 *Phys. Rev.* B **43** 9538
[27] Saha T and Mookerjee A 1996 *J. Phys.: Condens. Matter* **8** 2395
[28] Blügel S 1995 *Lectures in Magnetism on Surfaces* (Trieste: ICTP)